Effect of a SiO_2 layer on the thermal transport properties of ⟨100⟩ Si nanowires: A molecular dynamics study

Tomofumi Zushi
Faculty of Science and Engineering, Waseda University, 3-4-1 Ohkubo, Shinjyuku-ku, Tokyo 169-8555, Japan and Research Fellow of Japan Society for the Promotion of Science (JSPS), Japan

Kenji Ohmori and Keisaku Yamada
Graduate School of Pure and Applied Sciences, University of Tsukuba, 1-1-1 Tennodai, Tsukuba, Ibaraki 305-8577, Japan

Takanobu Watanabe
Faculty of Science and Engineering, Waseda University, 3-4-1 Ohkubo, Shinjyuku-ku, Tokyo 169-8555, Japan
(Received 10 November 2014; revised manuscript received 2 March 2015; published 18 March 2015)

The presence of a SiO_2 layer on Si nanowires (SiNWs) has been found through molecular dynamics simulation to reduce their thermal conductivity (κ), with κ approaching the amorphous limit of Si as the oxide layer thickness is increased. Through analysis of the phonon energy dispersion and vibrational density of states (VDOS) spectrum, this decrease in κ was attributed to dispersionless vibrational states that appear in the low energy range below 4 THz as a result of the lattice vibration of Si atoms near the SiO_2/Si interface. The SiO_2 layer also induced a low-frequency tail in the VDOS spectrum, the length of which was more closely correlated to the reduction in κ than the frequency-integrated value of the VDOS spectrum. These findings provide a more refined explanation for the decrease in κ than has been previously observed, and contribute to providing a greater understanding of the anomalistic vibration near the interface that is critical to determining the heat conductivity in nanoscale materials.

DOI: 10.1103/PhysRevB.91.115308 PACS number(s): 65.80.−g, 68.65.−k

I. INTRODUCTION

Silicon nanowires (SiNWs) [1] have attracted considerable attention as a promising building block for field-effect transistors (FETs) [2,3] and thermoelectric devices [4,5] by virtue of their low dimensionality. Moreover, when the Si crystal feature size is less than that of the phonon mean free path, the thermal conductivity (κ) is known to drop by as much as 10–100 times when compared to bulk Si [4–11]. This decrease in κ leads to a significant enhancement in the figure of merit (ZT) of thermoelectric materials [4,5], but is an unwelcome effect in nanoscale metal-oxide-semiconductor FETs [2,3] due to the increased device degradation caused by Joule heating. Thus, a greater understanding of this anomalous thermal conductivity is an important issue for the future development of Si nanodevices.

Past experimental studies have demonstrated that the κ of SiNWs is sensitive to the wire diameter [4,12,13] and surface roughness [4,14–17], with Li *et al.* [12] reporting that κ is suppressed by a factor of about 100 with respect to the bulk value when the wire diameter is reduced to $\sim$20 nm. Hochbaum *et al.* [5] have also shown that κ can be even further reduced by etching and roughening the wire surface by means of electroless etching (EE), while Hippalgaonkar *et al.* [14] identified that there is a less significant decrease in κ if SiNWs are fabricated by electron beam lithography rather than EE. A more detailed investigation into the relation between the κ and surface roughness of SiNWs conducted by Lim *et al.* [15] using high-resolution transmission electron microscopy revealed that the roughness power spectrum has a larger effect on κ than the diameter of the NW. Contrary to this, Feser *et al.* [13] concluded on the basis of Raman spectroscopy observation that the decrease in κ is instead caused by a change in the atomic structure introduced by etching, and not a roughening of the NW surface.

The decrease in the κ of low-dimensional materials has been explained by several theoretical models [18–27], which can be broadly divided into four classes. In the first model, hereafter referred to as model I, a decrease in the phonon group velocity due to the modification of the phonon energy dispersion is believed to lead to an increase in the phonon scattering rate, and therefore a decrease in κ [19,20,26,28]. The second model (model II) attributes the lower κ value to a phonon-boundary scattering effect that increases diffuse reflection on the surface of the material [21,22,25]. The significant role of boundary scattering is discussed, for example, in Refs. [10] and [18]. In the third model (model III), the decrease in κ is considered to originate from localized entrapment of phonons at a given position in the NW [8,9], as has been reported by Chen *et al.* [8]. Finally, more recent studies (model IV) have indicated that the presence of an amorphous silicon dioxide (SiO_2) film may influence κ [23,24], and that the change in the vibrational density of states (VDOS) at the SiO_2/Si interface is the more likely origin for the observed decrease [24].

Although all of the above mentioned models are based on solid theoretical grounds, respectively, the consensus about the major origin of the κ reduction has not yet been formed. This study therefore uses molecular dynamics (MD) simulation to investigate the most likely origin of the decrease in κ in SiNWs, with a particular focus on the relation between κ and phonon energy dispersion. The present work focuses on ⟨100⟩-oriented SiNWs, for which the κ reduction was observed experimentally [4,13]. This simulation model explicitly includes the SiO_2 surface film, which is known to induce considerable disorder in the Si lattice at the interface. It

 ©2015 American Physical Society

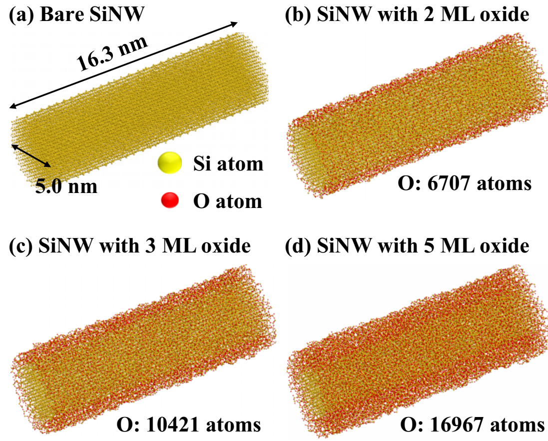

FIG. 1. (Color online) Molecular dynamics simulation models of a SiNW with (a) 0, (b) 2, (c) 3, or (d) 5 monolayers (ML) of oxide film.

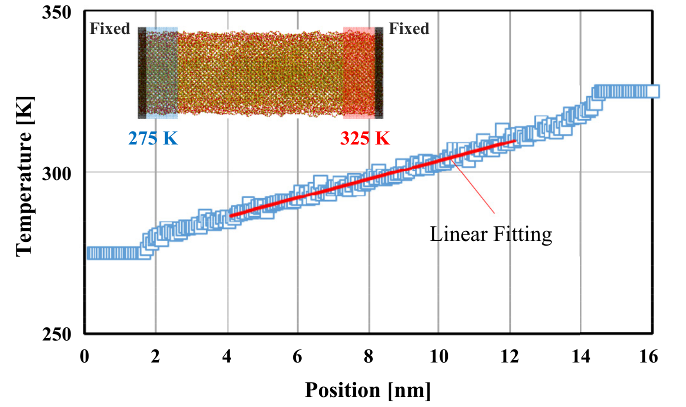

FIG. 2. (Color online) Temperature gradient along the length of a SiNW. A linear fit is shown by the red solid line.

is found that the presence of this oxide layer causes extra vibrational states, which appear as dispersionless phonon bands in the low energy range. We subsequently demonstrate that there is a quantitative correlation between the density of these dispersionless vibrational states and κ.

II. SIMULATION METHODS

Figure 1 shows simulation models for SiNWs with a $\langle 100 \rangle$ orientation and covered with an oxide film, which were formed from a bare cylindrical SiNW measuring 5.0 nm in diameter and 16.3 nm in length, and containing 15 870 Si atoms. An oxide layer was then added by inserting O atoms into the midpoints of the Si-Si bonds on the wire surface using a layer-by-layer manner. Insertion sites were randomly chosen from all of the Si-Si bonds at the interface, but the oxidation of the next layer was suppressed until the upper monolayer (ML) was fully oxidized. After each oxidation of 0.1 ML, the whole structure was optimized by a conjugate gradient method. Next, an MD calculation was performed at a temperature of 1000 K to further relax the whole structure by promoting the amorphization of the oxide film. Figures 1(b), 1(c), and 1(d) show the partially oxidized SiNW models with two, three, and five ML oxide films, respectively.

Thermal conductivity was calculated by means of nonequilibrium MD (NEMD) simulation [29–36], wherein fixed boundary conditions were imposed on both ends of the NW in its axis direction, but other surface atoms were free to move. First, we execute an NVT MD simulation for 1.0 ns at 300 K to equilibrate the whole system. Second, each end of SiNW are thermostated to 275 and 325 K, respectively, to form a cold and hot heat bath. The lengths of these heat bath regions were defined as 10% of the total wire length, and their temperature was controlled by the velocity scaling method [33–35]. The NEMD simulation was then conducted for a further 1.2 ns, which is sufficiently long enough to reach a steady-state condition and establish a constant temperature gradient (∇T) with a constant heat flux.

Figure 2 shows the temperature gradient established along the NW by the NEMD simulation, in which the temperature was calculated from the kinetic energy of the atoms and is time averaged over 0.2 ns. Using this temperature profile, ∇T is estimated by a linear fitting in order to calculate κ from Fourier's law: $\kappa = J/\nabla T$. Here the heat flux J is defined as the amount of energy transferred from the hot to cold bath regions over a given unit time through a unit cross sectional area.

To investigate the change in κ in relation to the phonon modes of the SiNW, the energy dispersion relation was calculated by a dynamical structure factor. The phonon dispersion relation is therefore obtained as ridges on the contour map of the dynamical structure factor S($\mathbf{k}$,ω), which is defined as

$$S(\mathbf{k},\omega) = \frac{1}{2\pi} \left| \int_0^T \rho(\mathbf{k},t) \exp(i\omega t) \right| dt, \tag{1}$$

where $\mathbf{k}$ is the wave vector, ω is the angular frequency, and T is the total simulation time. The Fourier component of the atom density $\rho(\mathbf{k},t)$ is defined as

$$\rho(\mathbf{k},t) = \sum_{j=1}^{N} \exp[-i\mathbf{k} \cdot \mathbf{r}_j(t)], \tag{2}$$

where N is the total number of atoms, and $\mathbf{r}_j(t)$ is the trajectory of atom j obtained from MD simulation. The MD simulation to calculate S($\mathbf{k}$,ω) was conducted for 50 ps at 300 K, with a periodic boundary condition adopted in the longitudinal direction of the system. The wave vector was specified as $(2\pi/a)(q,0,0)(0 < q < 1)$ in the first Brillouin zone, where a is the Si lattice constant (0.543 nm). Since the Fourier component in Eq. (2) contains the dot product of the coordinate of particles $\mathbf{r}_j(t)$ and the wave number vector $\mathbf{k}$, only the longitudinal modes are examined by S($\mathbf{k}$,ω). In order to extract the transverse modes, S($\mathbf{k}$,ω) was scanned along $\mathbf{k} = (2\pi/a)(q,0,0) + \mathbf{G}$, where $\mathbf{G}$ is a reciprocal lattice vector perpendicular to $\mathbf{k}$ and taken to be $\mathbf{G} = (2\pi/a)(0,2,0)$.

An interatomic potential was employed for mixed systems of Si and O [37,38], and was simply an extended version of the Stillinger-Weber potential [39]. This potential was designed to reproduce the SiO_2/Si system including compressively strained interfacial layers. In Refs. [40] and [41] it has been demonstrated that the potential reproduces qualitatively the phonon dispersion curve of bulk Si.

III. RESULTS AND DISCUSSION

A. Thermal conductivity of ⟨100⟩ SiNWs

The κ values calculated for various oxide thicknesses are plotted in Fig. 3 as a function of the total cross-sectional area of the NW. We can see from this that the κ of a bare SiNW is 7.6 W/mK, which is 5% the value of bulk Si (156 W/mK) [42]. Furthermore, this calculated value agrees well with a previous report by Saegusa *et al.* [23], in which the κ of a SiNW 9.41 nm long and 4.84 nm diameter was estimated to be 6.6 W/mK. The slight variation between the two different calculations is reasonable in the light of the remark by Volz and Chen [10] that κ is independent of the NW length when it is longer than 8.7 nm. Figure 3 also shows that the κ of a SiNW reduces as the Si layer thickness is reduced by the growth of oxide layers, and approaches the amorphous limit of ∼1.0 W/mK for Si.

The decrease in κ is more significant than would be expected based on a simple estimation of the area ratio of the Si core to SiO_2 film. For instance, if we assume that the κ of a SiO_2-coated SiNW structure can be expressed by the weighted average of κ_{Si} and $\kappa_{\mathrm{SiO_2}}$ with cross-sectional area [32], then

$$\kappa = \frac{A_{\mathrm{Si}}}{A_{\mathrm{Si}} + A_{\mathrm{SiO_2}}}\kappa_{\mathrm{Si}} + \frac{A_{\mathrm{SiO_2}}}{A_{\mathrm{Si}} + A_{\mathrm{SiO_2}}}\kappa_{\mathrm{SiO_2}}. \quad (3)$$

This simple estimate is also shown in Fig. 3. Here κ_{Si} is assumed to be the thermal conductivity of bare SiNW of 7.6 W/m. The $\kappa_{\mathrm{SiO_2}}$ is assumed to range between 1.0 and 2.0 W/mK [23]. Note that this simple calculation tends to overestimate κ. This indicates that the decrease in κ with increasing oxide layer thickness cannot simply be explained by the reduction in area ratio between the thermally conducting Si core and thermally insulating oxide film, i.e., there are other factors responsible for reducing the thermal conductivity of SiNW covered with oxide film.

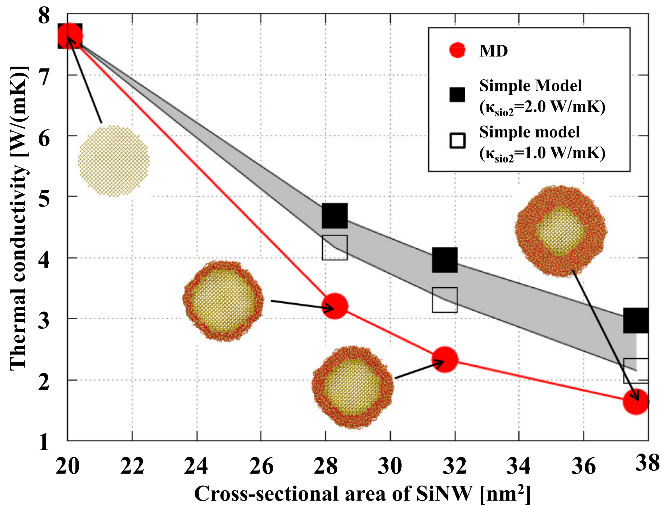

FIG. 3. (Color online) (a) Thermal conductivity κ of a SiNW as a function of its cross-sectional area. Solid circles represent κ values obtained by molecular dynamics simulation. Filled and open squares represent a simple estimation of κ with a $\kappa_{\mathrm{SiO_2}}$ of 1.0 and 2.0 W/mK, respectively. The shaded area is the model prediction with $1.0 < \kappa_{\mathrm{SiO_2}} < 2.0$ W/mK, in which κ_{Si} is assumed to be equal to the κ of bare SiNW (7.6 W/mK).

It is worth noting that, in our previous work [41], it was demonstrated that the heat diffusion is retarded by thinning the inner Si layer and is less dependent on the thickness of the outer SiO_2 layer. The result suggests that the κ decrease observed in the present work is mainly attributed to the thinning of the Si core rather than the increase of the oxide thickness.

B. Effect of a SiO_2 layer on phonon energy dispersion in SiNWs

Figures 4(a) and 4(b) show the intensity of the dynamical structure factor $S(\mathbf{k},\omega)$ for the whole body of a SiNW with various oxide thicknesses along $\mathbf{k} = (2\pi/a)(q,0,0)$ and $\mathbf{k} = (2\pi/a)(q,2,0)$, respectively. Note that a longitudinal acoustic (LA) phonon branch can be seen in Fig. 4(a), whereas a transverse acoustic (TA) phonon branch is evident in Fig. 4(b). In both figures, however, new dispersionless states appear in the low-energy region below 4.0 THz, which become increasingly more significant as the oxide thickness increases.

Figure 5 shows the intensity profile for $S(\mathbf{k},\omega)$ at $\mathbf{k} = (2\pi/a)(0.5,0,0) + \mathbf{G}$, in which the intensity peak at 4.8 THz corresponds to the TA phonon mode. This reveals that although the intensity of the TA mode decreases with increasing SiO_2 layer thickness, the broad spectra of the dispersionless vibrational states in the low-energy range below 4.0 THz actually increase. Given that low energy phonon modes are known to be responsible for heat conduction, the dispersionless phonon states induced by the outer SiO_2 film are considered to directly affect the heat conductivity of a SiNW.

Figure 6(a) shows the intensity of the dynamical structure factor $S(\mathbf{k},\omega)$ for the whole body of a SiNW with a 3 ML oxide layer, while Figs. 6(b) and 6(c) show the intensity for the Si core and interfacial Si region, respectively. It should be noted here that the Si core is defined as the Si atoms located 11th to 13th atomic layers from the surface, whereas the interfacial Si region represents the second to fourth layers. The superimposing of the LA and TA acoustic phonon branches on the same color map in Fig. 6 reveals that the intensity of the dispersionless states is most significant in the interfacial Si region. These dispersionless phonon states are therefore considered to be the result of the peculiar vibration of Si atoms near the SiO_2/Si interface; however, it is difficult to define their group velocity, effective mass, or lifetime [43]. This implies that the heat transfer properties of a SiNW surrounded by an oxide film cannot be discussed in the context of conventional harmonic oscillator approximation.

C. Vibrational density of states

Figure 7 shows the VDOS of the SiNWs, which was calculated by a Fourier transform of the atomic velocity correlation function [24,40]. The effect of the oxide film is reflected by the whole body fading of the VDOS spectra, which is attributed to the attenuation of bulklike phonon vibration modes. The appearance of the dispersionless phonon states is evidenced by the increase in the VDOS at frequencies below 4.0 THz, as shown in the inset of Fig. 7(a).

As shown in Figs. 7(b) and 7(c), a partial VDOS was calculated for the same Si core and interfacial Si regions that were defined in Fig. 6. As can be seen in Fig. 7(b), the partial VDOS of the Si core is almost identical to that of a bare NW,

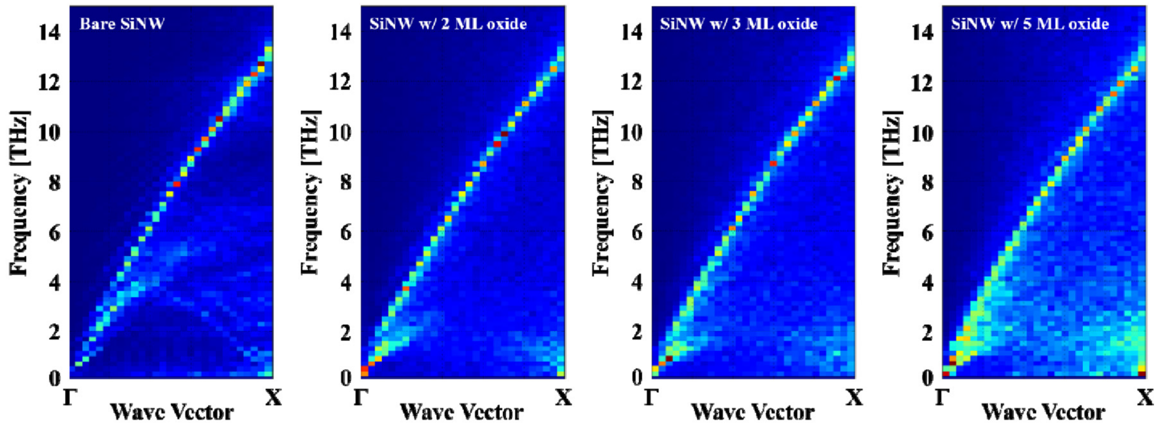

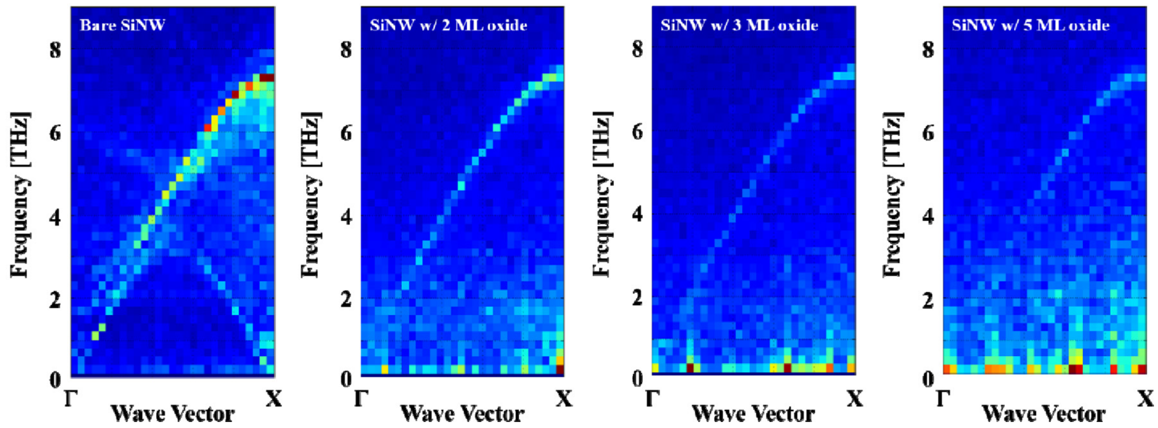

FIG. 4. (Color online) Phonon dispersion relation of acoustic phonon modes. (a) Longitudinal and (b) transverse acoustic mode of a SiNW with 0, 2, 3, or 5 monolayers of oxide film.

which means that the vibrational properties are unchanged even if the NW is covered with a SiO_2 oxide film. In contrast, the VDOS of the interfacial Si region is attenuated over a wide frequency range as the oxide thickness increases, which is consistent with a previous evaluation of the VDOS of a SiNW embedded in a silica matrix by He and Galli [24]. In the low-energy range below 4 THz, however, the VDOS increases with oxide thickness, which of course corresponds to the appearance of dispersionless states in the dynamical structural factor.

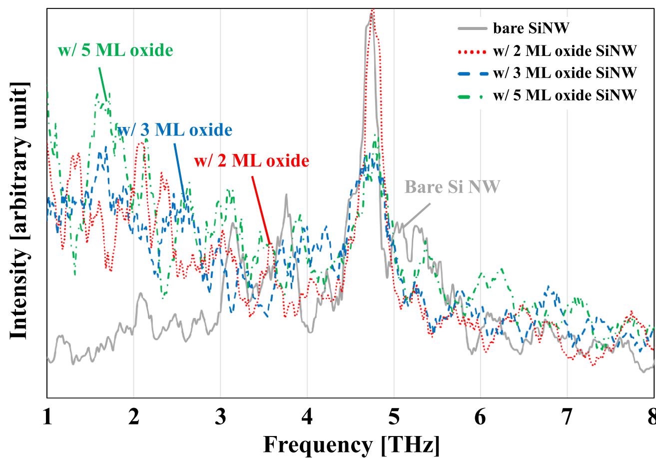

FIG. 5. (Color online) Intensity of the dynamical structure factor as a function of frequency for a SiNW with 0, 2, 3, or 5 monolayers of oxide film. The wave vector is $(2\pi/a)(0.5,0,0)$.

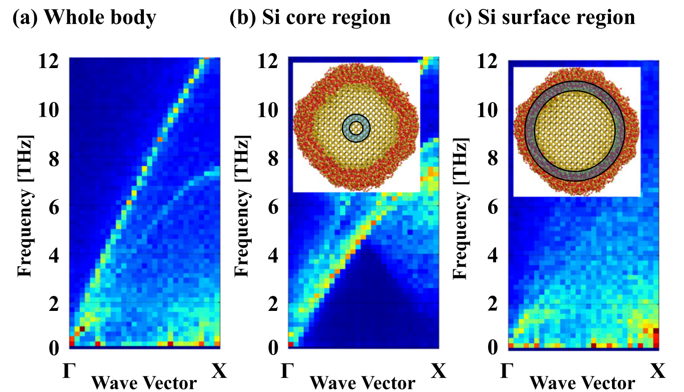

FIG. 6. (Color online) Partial dynamical structure factor of a SiNW covered with 3 monolayers of oxide. (a) Whole body, (b) Si core encompassing the 11th to 13th atomic layers from the surface, and (c) the Si surface region between the second and fourth atomic layers.

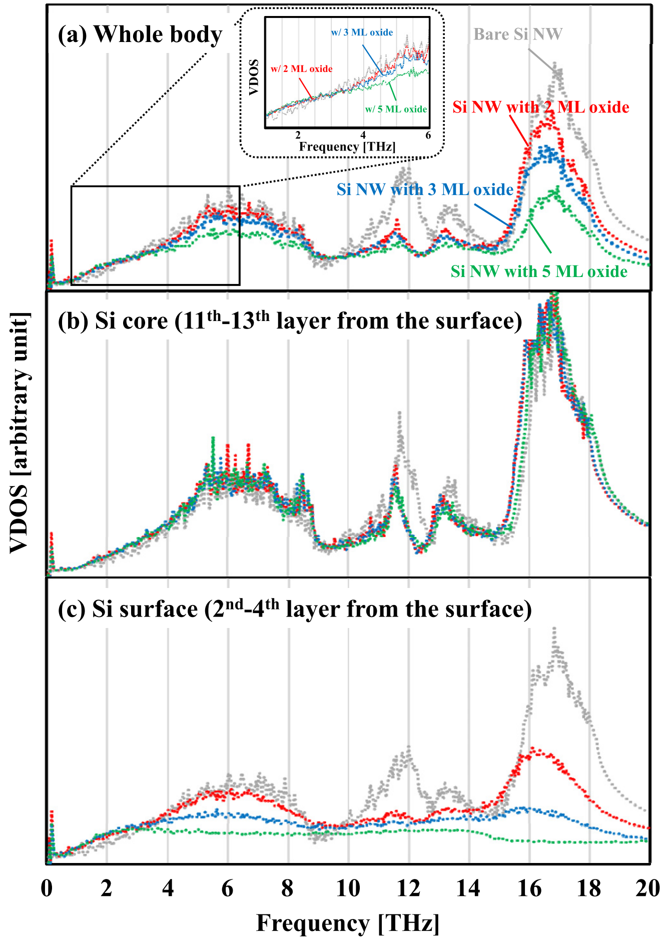

FIG. 7. (Color online) Vibrational density of states for bare and oxidized SiNWs. (a) Whole body, (b) Si core region (11th to 13th atomic layer from the surface), and (c) Si surface region (second to fourth atomic layer).

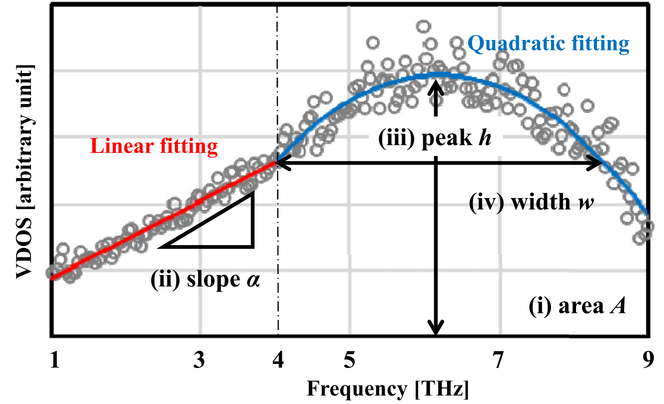

FIG. 8. (Color online) Illustration of the four VDOS parameters used to characterize its shape: (i) area, (ii) slope, (iii) peak, and (iv) width of the VDOS curve. The VDOS curve was fitted at lower frequencies (1.0–4.0 THz) by a linear function, but a quadratic function was used at higher frequencies (4.0–9.0 THz).

In order to better clarify the impact of the new dispersionless states at the SiO_2/Si interface on κ, the correlation between the VDOS shape of acoustic phonons and κ was investigated. For this, the VDOS shape in the energy range between 1.0 and 9.0 THz was characterized by four parameters, as shown in Fig. 8: (i) the area under the VDOS curve A, (ii) the tail slope α of the VDOS in the low-frequency region below 4.0 THz, (iii) the peak value h, and (iv) the full-width at half maximum w. Figures 9(a)–9(d) shows the κ of a SiNW and each of these four parameters, with α clearly exhibiting the closest correlation. In other words, κ decreases with the slope of the low-frequency tail of VDOS, whereas the length of the low-frequency tail corresponds to the dispersionless states. This means that the decrease in κ observed in SiNWs can be attributed to the appearance of new vibrational states near the SiO_2/Si interface, as opposed to the attenuation of the frequency-integrated value of the VDOS spectrum.

D. The κ reduction mechanism

The appearance of dispersionless states in SiNW offers a more refined explanation for the observed decrease in κ than the previously proposed mechanisms outlined in Sec. I. For example, since the group velocity cannot be defined for the dispersionless phonon states shown in Fig. 4, model I clearly does not provide an adequate explanation. The appearance of these dispersionless phonons does indicate an enhanced phonon scattering at the interface that is concordant with model II; however, the present results also suggest that this phonon scattering is enhanced by randomly distributing these dispersionless states at the interface, and not by increasing the interfacial roughness. Thus, the significant decrease in κ cannot be explained quantitatively by only considering the elastic phonon scattering at a roughened SiO_2/Si interface [25]. Furthermore, as shown in Fig. 9, the decrease in κ is more closely correlated to the enhancement of dispersionless states than any decrease in VDOS, which means that model IV also fails to indicate the direct origin of the κ reduction.

Model III, which is based on phonon localization at the surface, is therefore the one that most closely matches with the results of this study. This would mean that the oxide-induced dispersionless states have no clear dependency on the wave vector $\mathbf{k}$, and that vibrational state does not propagate systematically in any given direction. However, as shown in Fig. 4, the oxide-induced states appear as noise, and so vibration is clearly not strictly localized at a specific position. Thus, nonpropagative vibrations at the SiO_2/Si interface are likely to disturb the heat transfer, making the appearance of the random dispersionless states responsible for the observed decrease in κ. We note that, although our results are obtained for $\langle 100 \rangle$-oriented SiNW, it is expected that the anomalous κ behavior induced by the atomistic disorders can be observed in other crystal orientations. This point is open for future studies.

It is worth noting here that lattice disorder near the SiO_2/Si interface is known to hinder the current flow of narrow SiNW transistors [44]. Moreover, the phonon properties near the SiO_2/Si interface are considered to be significantly affected by the interfacial lattice disorder, meaning that the force constant of the Si lattice must be modified near the SiO_2/Si interface. Given this, the anomalous properties of carrier and heat transport in nanostructured materials can be attributed to the atomic structure of the interface, thus making control over

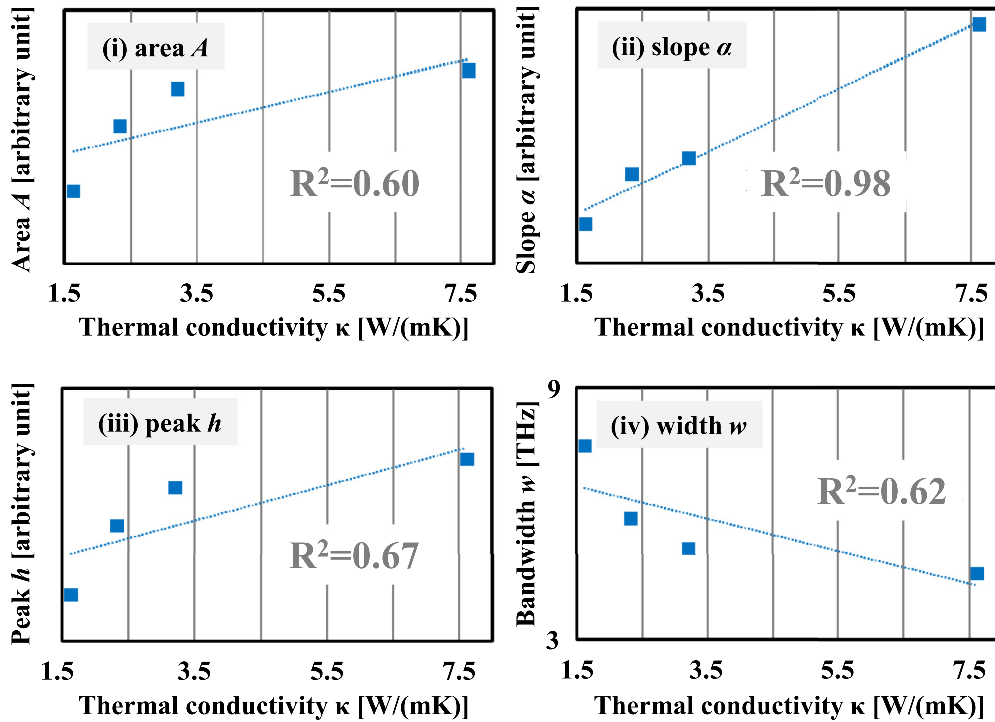

FIG. 9. (Color online) Dependence of κ on the (i) area, (ii) slope, (iii) peak, and (iv) width of the VDOS curve. The coefficient of determination R^2 is also shown in each graph.

this interface at an atomic scale essential to improving the thermoelectric properties of practical Si nanodevices.

IV. CONCLUSIONS

Evaluation of the oxide thickness dependence of κ in SiNWs by NEMD simulation has demonstrated that κ decreases with increasing oxide thickness increases, and approaches the amorphous limit for Si. This decrease in κ cannot be simply explained by the reduction in area ratio of the heat-conductive Si core to the heat resistive SiO_2 film, but rather is attributed to newly generated dispersionless phonon states near the SiO_2/Si interface. Thus, the decrease in κ is more closely correlated with the extent of the low-frequency tail of VDOS than the frequency integral. It is therefore concluded that modification of the vibrational properties near this interface is essential to understanding heat conduction in low-dimensional materials.

ACKNOWLEDGMENTS

This work was supported by a Grant-in-Aid for Scientific Research (B) (Grant No. 24310082) from the Ministry of Education, Culture, Sports, Science and Technology, Japan. It is also acknowledged that T. Zushi is a research fellow of the Japan Society for the Promotion of Science. We acknowledge the Tsukuba Nanotechnology Human Resource Development Program, University of Tsukuba.

[1] R. Rurali, Rev. Mod. Phys. **82**, 427 (2010).
[2] J. Chen, T. Saraya, and T. Hiramoto, in *2010 Symposium on VLSI Technology (VLSIT)* (IEEE, Washington, DC, 2010), pp. 175–176.
[3] H. Iwai, ECS Trans. **50**, 251 (2013).
[4] A. I. Boukai, Y. Bunimovich, J. Tahir-Kheli, J.-K. Yu, W. A. Goddard Iii, and J. R. Heath, Nature (London) **451**, 168 (2008).
[5] A. I. Hochbaum, R. Chen, R. D. Delgado, W. Liang, E. C. Garnett, M. Najarian, A. Majumdar, and P. Yang, Nature (London) **451**, 163 (2008).
[6] J. Heron, T. Fournier, N. Mingo, and O. Bourgeois, Nano Lett. **9**, 1861 (2009).
[7] I. Ponomareva, D. Srivastava, and M. Menon, Nano Lett. **7**, 1155 (2007).
[8] J. Chen, G. Zhang, and B. Li, Nano Lett. **10**, 3978 (2010).
[9] J. Chen, G. Zhang, and B. Li, J. Chem. Phys. **135**, 204705 (2011).
[10] S. G. Volz and G. Chen, Appl. Phys. Lett. **75**, 2056 (1999).
[11] K. Kukita, I. N. Adisusilo, and Y. Kamakura, Jpn. J. Appl. Phys. **53**, 015001 (2014).
[12] D. Li, Y. Wu, P. Kim, L. Shi, P. Yang, and A. Majumdar, Appl. Phys. Lett. **83**, 2934 (2003).
[13] J. P. Feser, J. S. Sadhu, B. P. Azeredo, K. H. Hsu, J. Ma, J. Kim, M. Seong, N. X. Fang, X. Li, P. M. Ferreira *et al.*, J. Appl. Phys. **112**, 114306 (2012).
[14] K. Hippalgaonkar, B. Huang, R. Chen, K. Sawyer, P. Ercius, and A. Majumdar, Nano Lett. **10**, 4341 (2010).
[15] J. Lim, K. Hippalgaonkar, S. C. Andrews, A. Majumdar, and P. Yang, Nano Lett. **12**, 2475 (2012).

[16] M. Ghossoub, K. Valavala, M. Seong, B. Azeredo, K. Hsu, J. Sadhu, P. Singh, and S. Sinha, Nano Lett. **13**, 1564 (2013).

[17] C. Blanc, A. Rajabpour, S. Volz, T. Fournier, and O. Bourgeois, Appl. Phys. Lett. **103**, 043109 (2013).

[18] N. Mingo, Phys. Rev. B **68**, 113308 (2003).

[19] A. Balandin and K. L. Wang, J. Appl. Phys. **84**, 6149 (1998).

[20] M. Stroscio, Y. M. Sirenko, S. Yu, and K. Kim, J. Phys.: Condens. Matter **8**, 2143 (1996).

[21] Y.-R. Chen, M. S. Jeng, Y. W. Chou, and C. C. Yang, Comput. Mater. Sci. **50**, 1932 (2011).

[22] L. Liu and X. Chen, J. Appl. Phys. **107**, 033501 (2010).

[23] T. Saegusa, K. Eriguchi, K. Ono, and H. Ohta, Jpn. J. Appl. Phys. **49**, 095204 (2010).

[24] Y. He and G. Galli, Phys. Rev. Lett. **108**, 215901 (2012).

[25] P. Martin, Z. Aksamija, E. Pop, and U. Ravaioli, Phys. Rev. Lett. **102**, 125503 (2009).

[26] M. Luisier, J. Appl. Phys. **110**, 074510 (2011).

[27] D. Donadio and G. Galli, Phys. Rev. Lett. **102**, 195901 (2009).

[28] T. Markussen, A.-P. Jauho, and M. Brandbyge, Phys. Rev. B **79**, 035415 (2009).

[29] M. Hu, K. P. Giapis, J. V. Goicochea, X. Zhang, and D. Poulikakos, Nano Lett. **11**, 618 (2011).

[30] J. Chen, G. Zhang, and B. Li, Nano Lett. **12**, 2826 (2012).

[31] S.-c. Wang, X.-g. Liang, X.-h. Xu, and T. Ohara, J. Appl. Phys. **105**, 014316 (2009).

[32] Y. Gao, W. Bao, Q. Meng, Y. Jing, and X. Song, J. Non-Cryst. Solids **387**, 132 (2014).

[33] Z. Huang and Z. Tang, Physica B (Amsterdam) **373**, 291 (2006).

[34] S.-H. Choi, S. Maruyama, K.-K. Kim, and J.-H. Lee, J. Korean Phys. Soc. **43**, 747 (2003).

[35] A. Cummings, M. Osman, D. Srivastava, and M. Menon, Phys. Rev. B **70**, 115405 (2004).

[36] P. K. Schelling, S. R. Phillpot, and P. Keblinski, Phys. Rev. B **65**, 144306 (2002).

[37] T. Watanabe, K. Tatsumura, and I. Ohdomari, Appl. Surf. Sci. **237**, 125 (2004).

[38] T. Watanabe, T. Onda, and I. Ohdomari, ECS Trans. **33**, 901 (2010).

[39] F. H. Stillinger and T. A. Weber, Phys. Rev. B **31**, 5262 (1985).

[40] T. Zushi, K. Shimura, M. Tomita, K. Ohmori, K. Yamada, and T. Watanabe, ECS J. Solid State Sci. Technol. **3**, P149 (2014).

[41] T. Zushi, Y. Kamakura, K. Taniguchi, I. Ohdomari, and T. Watanabe, Jpn. J. Appl. Phys. **50**, 010102 (2011).

[42] C. Glassbrenner and G. A. Slack, Phys. Rev. **134**, A1058 (1964).

[43] N. Ashcroft and N. Mermin, *Solid State Physics* (Thomson Learning, London, 1976).

[44] H. Minari, T. Zushi, T. Watanabe, Y. Kamakura, S. Uno, and N. Mori, in *2011 Symposium on VLSI Technology (VLSIT)* (IEEE, Washington, DC, 2011), pp. 122–123.